ELSEVIER

Alzheimer's & Dementia 10 (2014) e19–e26

Alzheimer's & Dementia

Cortical phase changes in Alzheimer's disease at 7T MRI: A novel imaging marker

Sanneke van Rooden[a,c,*], Maarten J. Versluis[a], Michael K. Liem[c], Julien Milles[b], Andrea B. Maier[d], Ania M. Oleksik[d], Andrew G. Webb[a], Mark A. van Buchem[a,c], Jeroen van der Grond[a,c]

[a]*C.J. Gorter Center for High-Field MRI, Leiden University Medical Center, Leiden, The Netherlands*
[b]*Division of Image Processing, Leiden University Medical Center, Leiden, The Netherlands*
[c]*Department of Radiology, Leiden University Medical Center, Leiden, The Netherlands*
[d]*Department of Gerontology and Geriatrics, Leiden University Medical Center, Leiden, The Netherlands*

Abstract

Background: Postmortem studies have indicated the potential of high-field magnetic resonance imaging (MRI) to visualize amyloid depositions in the cerebral cortex. The aim of this study is to test this hypothesis in patients with Alzheimer's disease (AD).

Methods: T2*-weighted MRI was performed in 16 AD patients and 15 control subjects. All magnetic resonance images were scored qualitatively by visual assessment, and quantitatively by measuring phase shifts in the cortical gray matter and hippocampus. Statistical analysis was performed to assess differences between groups.

Results: Patients with AD demonstrated an increased phase shift in the cortex in the temporoparietal, frontal, and parietal regions ($P < .005$), and this was associated with individual Mini-Mental State Examination scores ($r = -0.54$, $P < .05$).

Conclusion: Increased cortical phase shift in AD patients demonstrated on 7-tesla T2*-weighted MRI is a potential new biomarker for AD, which may reflect amyloid pathology in the early stages.

Keywords: Alzheimer's disease; Brain imaging; Human 7T MRI; AD pathology; Phase changes; Biomarker

1. Introduction

Alzheimer's disease (AD) can only be diagnosed with certainty at autopsy, based on the histological detection of senile plaques containing fibrillary amyloid beta (Aβ) and neurofibrillary tangles. Currently, because of the absence of validated sensitive and specific tests, the clinical diagnosis of AD can only be made at a late stage of disease progression and with a considerable degree of uncertainty—probable AD, at best—and is based on criteria from the Diagnostic and Statistical Manual of Mental Disorders, 4th edition, and the National Institute of Neurological, Communicative Disorders and Stroke–Alzheimer's Disease and Related Disorders Association. Nevertheless, the histological hallmarks of AD pathology, comprising amyloid plaques and neurofibrillary tangles, are known to occur up to 10 to 20 years before the objective detection of cognitive decline [1]. Recently, positron emission tomography (PET) using Pittsburgh compound B (PiB) has been introduced as a diagnostic tool to detect cerebral amyloid in vivo [2–8]. The major disadvantages of PiB-PET are the need to use a radioactive tracer, the relative scarcity of institutions that can perform such scans because of the requirement for an onsite cyclotron, the inability to acquire anatomic and functional information in the brain during the same examination, and the greater chance of false positives, making interpretation of PiB-PET scans more difficult, especially in the elderly, which hampers the use of this method as a diagnostic tool in the elderly [9].

Earlier research demonstrated the potential of high-field (7T) magnetic resonance imaging (MRI) in the diagnosis of AD by showing distinct intensity changes in the cortex on T2*-weighted images of postmortem brain specimens of AD patients. These features included hypointense foci and diffuse granular patterns of less distinct hypointense foci in the cerebral cortex [10]. Similar patterns have been

*Corresponding author. Tel.: +31-71-5264376; Fax: +31-71-5248256.
E-mail address: S.van_Rooden@lumc.nl

1552-5260/$ - see front matter
http://dx.doi.org/10.1016/j.jalz.2013.02.002

described in studies of AD transgenic mice and postmortem human AD cases, and were attributed to the presence of amyloid plaques using histological confirmation [11–19]. It has been proposed that the visualization on MRI of plaques in humans and mice is based on the fact that these deposits colocalize with iron, which gives rise to magnetic susceptibility effects on T2*-weighted images over volumes that are much larger than the actual size of amyloid plaques [17,19–24]. An alternative method to measure these susceptibility changes in the brain is to measure the relative phase in regions of interest (ROIs), because it has been shown that this is a reliable indicator of the iron content in the brain [25–28]. Although previous studies have demonstrated the potential of this approach in high-field MRI [29,30], no clinical studies have been performed yet on AD patients in vivo for the detection of AD pathology.

The overall aim of the current study is to confirm previous postmortem findings by detecting AD pathology in the cerebral cortex and hippocampus using a novel, in vivo, 7T high-field magnetic resonance (MR) approach.

2. Materials and methods

2.1. Participants

This study was approved by the local institutional review board. In all cases, informed consent was obtained according to the declaration of Helsinki [31]. In total, 16 AD patients with a mean age of 76.9 years (range, 68–86 years; 10 male/6 female) and 15 control subjects with a mean age of 75.1 years (range, 69–80 years; 10 male/5 female) were included.

The AD patients were recruited from the memory clinic of the Leiden University Medical Center. Memory clinic patients were referred to the hospital by their general practitioner or a medical specialist. Prior to the 7T study, these patients all underwent a routine clinical protocol comprising a whole-brain MRI (3T), a battery of neuropsychological tests, and a general medical and neurological examination performed by a neurologist, psychiatrist, or internist–geriatrician. The diagnosis was made in a multidisciplinary consensus meeting using the National Institute of Neurological, Communicative Disorders and Stroke–Alzheimer's Disease and Related Disorders Association criteria for diagnosing probable AD [32]. Participants with the diagnosis of probable AD who were capable of giving informed consent (Mini-Mental State Examination (MMSE) score $\geq$19 points) with late-onset dementia (age $>$67 years) were selected for inclusion in the 7T study either retrospectively within 1 year after attending the memory clinic, or prospectively. Only patients with a "pure" form of AD were selected. Patients categorized as having a mixed form of dementia, or cerebral amyloid angiopathy (CAA), were not included in the study. Patients showing hemorrhagic lesions on T2*-weighted 3T MRI and/or diagnosed as possible or probable CAA according to the Boston criteria [33] were excluded.

Healthy control subjects were recruited by focused advertisement. Subjects with an age between 69 years and 80 years who were living independently, had an MMSE score $\geq$25 points, and had a Geriatric Depression Scale score $\leq$4 points were selected for inclusion. Subjects were screened by an internist–geriatrician (including for any cognitive deficits), and subjects with the following diseases were excluded: hemorrhagic and ischemic stroke, Morbus Parkinson, dementia, mild cognitive impairment, diabetes mellitus, rheumatoid arthritis, polymyalgia rheumatica, cancer, heart failure, and chronic obstructive pulmonary disease.

2.2. MRI

2.2.1. Image acquisition

MRI was performed on a whole-body human 7T MR system (Philips Healthcare, Best, The Netherlands) using a quadrature transmit and 16-channel receive head coil (Nova Medical, Wilmington, MA). Participants were scanned using a two-dimensional (2D), flow-compensated, transverse T2*-weighted gradient echo scan that included the frontal and parietal regions for amyloid detection with a total imaging duration of 10 minutes. Positioning of this stack was done on the sagittal plane of the survey within the frontal and parietal region above the occipital lobe. The middle of the stack was positioned through the corpus callosum, just above the thalamus. Fig. 1 shows a typical positioning of these 20 slices. Imaging parameters were repetition time/echo time, 794/25 ms; flip angle, 45°; slice thickness, 1.0 mm with a 0.1-mm interslice gap; number of slices, 20; field of view, 240 $\times$ 180 $\times$ 22 mm; and matrix size, 1000 $\times$ 1024; resulting in an in-plane nominal spatial resolution of 0.24 $\times$ 0.24 mm^2. The bandwidth per pixel was 46 Hz, corresponding to a readout length of approximately 22 ms. The frequency and phase-encoding directions were

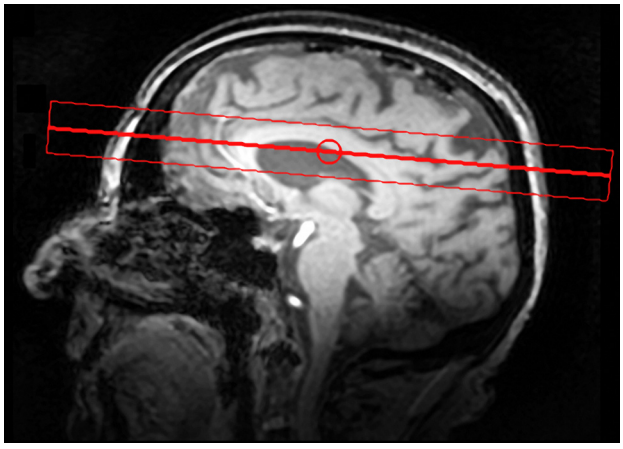

Fig. 1. Survey image on which the stack position of the two-dimensional T2*-weighted gradient echo scan, including the frontal and parietal cortex for amyloid detection, is shown. Image shows sagittal plane.

along the anterior–posterior and right–left axes, respectively. In addition, a coronal, 2D, flow-compensated T2*-weighted gradient echo scan covering the hippocampus, with a total imaging duration of 6 minutes, was performed. Positioning of this stack was done on a T1-weighted image in sagittal and coronal orientation. The stack was placed parallel to and partly over the brainstem, and in front of it on the sagittal T1-weighted image. Based on the T1-weighted images in the coronal orientation, it was checked whether the stack included the head of the hippocampus. Imaging parameters were repetition time/echo time, 624/14 ms; flip angle, 40°; slice thickness, 3.0 mm with no interslice gap; number of slices, 32; field of view, 240 × 180 × 96 mm; and matrix size, 480 × 480; resulting in a nominal in-plane spatial resolution of 0.5 × 0.5 mm^2. These sequences are very sensitive to image artifacts arising from resonance frequency fluctuations within the brain caused by slight patient movements, even in areas significantly away from the head. A navigator echo was included to correct for these artifacts [34]. Shimming up to third order was performed using an image-based shimming approach [35]. The phase images were subsequently unwrapped by high-pass filtering with a 92 × 92 kernel size [36].

2.2.2. Image analysis

First, the T2*-weighted gradient echo images were evaluated, blinded for diagnosis, for hypointense foci by S. v. R. and checked by M. v. B. as described in a previous ex vivo study [10].

Image phase values in the cortex were determined using the transverse 2D T2*-weighted gradient echo scans. Based on the visual observation on unwrapped phase images of a higher contrast between gray and white matter in AD patients than in control subjects, resulting from a higher signal intensity within the gray matter, the phase values of the cortical gray matter were determined in ROIs in four different areas of the brain—temporoparietal left, temporoparietal right, frontal, and parietal—which were positioned according a detailed human brain atlas. Because of the laminar variation in the cortical areas [29], histograms perpendicular to the cortex within these regions were created to measure peak gray matter phase values, over at least 10 cortical regions per slice and per region. To correct for local macroscopic magnetic field inhomogeneities subcortical white matter phase values were measured and used as an internal reference value. Phase values for gray and white matter were measured in these four areas per MRI slice for every other slice (10 in total), resulting in 40 phase values for gray and white matter separately per subject. Phase values of the different ROIs of the four regions were averaged. Per subject, the overall phase shift between cortical gray matter and subcortical white matter (cortical phase shift) was calculated for each region and expressed in radians.

Phase values of the hippocampus were determined using the coronal 2D T2*-weighted gradient echo scans. The hippocampus was segmented manually, and phase values were determined on five consecutive slices, starting at the head of the hippocampus, for the right and left hippocampus separately. The slice showing the red nucleus most pronounced was used as the middle slice for drawing an ROI, and the two slices in front and after this slice were used to select the ROIs. For each subject, these five measurements were averaged for each hippocampus. Phase values of the white matter were determined in three neighboring areas of subcortical white matter on each of the five slices and averaged per subject. The phase shift of the hippocampus was calculated by the difference in phase value of the hippocampus and white matter (hippocampal phase shift) and expressed in radians. Analysis of the hippocampus was performed only in 12 of the 16 AD patients and in 14 of the 15 control subjects because of severe motion artifacts that could not be corrected completely (three subjects) or because participants were not able to finish the whole scan protocol (two subjects).

2.3. Statistics

A Mann–Whitney *U* test was used to assess differences in age, gender, MMSE score, and phase measurements between AD and control groups. Logistic regression analysis was used to assess the association between diagnosis and intertissue phase shifts in the cortex and hippocampus, corrected for age and gender. To assess the interaction between cortical gray matter/hippocampal and white matter phase values, both were also entered as covariates in one model. Receiver operating characteristic (ROC) analysis was performed to determine the area under the ROC curve and to assess the optimal cutoff phase shift in the cortex and hippocampus to detect AD with its corresponding sensitivity, specificity, positive predictive value, and negative predictive value. To determine the association between MMSE and phase shift in the cortex and hippocampus, a linear regression analysis including a Pearson correlation corrected for age and gender was performed. All statistical analyses were performed with the Statistical Package of Social Sciences (SPSS, version 17.0.1; SPSS, Chicago, IL).

3. Results

The characteristics of the participants are shown in Table 1. No difference in age or gender was found between patient and control groups. Scores for global cognitive functioning (MMSE score) were significantly higher in control subjects (29.0 points) than in patients with AD (22.5 points; $P < .001$).

Fig. 2 shows representative, transverse T2*-weighted magnitude and phase images of the parietal cortex of a subject with AD (Fig. 2A, B) and a control subject (Fig. 2C, D). Fig. 3 shows coronal T2*-weighted magnitude and phase images of the hippocampus of a subject with AD (Fig. 3A, B) and a control subject (Fig. 3C, D). In none of the subjects

Table 1
Characteristics of AD patients and control subjects

Variables	AD (n = 16)	Control (n = 15)
Mean age, years (range)	76.9 (68–86)	75.1 (69–80)
Male/female, n	10/6	10/5
Median MMSE score, points (range)	22.5 (19–26)	29.0 (27–30)

Abbreviations: AD, Alzheimer's disease; MMSE, Mini-Mental State Examination.

were small, focal hypointensities found in either the cortex or hippocampus.

Table 2 shows the mean phase shifts of the temporoparietal, frontal, parietal cortex, and the right and left hippocampus. For the temporoparietal, frontal, and parietal cortex, a larger cortical phase shift ($P < .005$) was found in the AD patients compared with control subjects (adjusted for age and gender). For both hippocampi, no difference in phase shifts between groups was observed. Analysis in which both gray matter and white matter values were entered in the logistic regression model showed that only the cortical gray matter phase value, and not the white matter phase value, was associated with diagnosis. For the hippocampus, both gray and white matter phase values were not associated with diagnosis.

To determine the diagnostic value of the phase measurements in differentiating AD from control subjects, ROC analysis was performed for each region. Table 3 shows the area under the curve (AUC), cutoff value, sensitivity, specificity, and positive and negative predictive values of all regions selected. For the temporoparietal, frontal, and parietal cortex, an AUC between 0.79 and 0.85 was found, with the regions all having a high specificity (90%–100%) and a moderate to high sensitivity (50%–70%). Of these regions, the parietal cortex demonstrated the highest AUC (0.85), with a sensitivity of 69% and a specificity of 93%. The corresponding positive predictive value and negative predictive value were 92% and 74%, respectively. Both hippocampi demonstrated a lower AUC (right hippocampus, 0.66; left hippocampus, 0.67), which resulted in a relatively lower specificity and positive predictive value. The sensitivity and negative predictive values were comparable with the regions in the cortex.

There was a significant negative correlation (adjusted for age and gender) between MMSE score and phase shift in the left temporoparietal cortex ($r = -0.47$, [$\beta = -0.464$, $P < .05$]), the right temporoparietal cortex ($r = -0.41$, [$\beta = -0.473$, $P < .05$]), frontal cortex ($r = -0.44$, [$\beta = -0.404$, $P < .05$]), and parietal cortex ($r = -0.54$, [$\beta = -0.501$, $P < .05$]; all, $P < .05$). For the right and the left hippocampus, there was no correlation between MMSE score and phase shift (right hippocampus, $r = -0.25$, $P = .21$ [$\beta = -0.168$, $P = .404$], left hippocampus, $r = -0.27$, $P = .19$ [$\beta = -0.190$, $P = .336$]).

4. Discussion

The first initial results of this study show that, using a novel high-field imaging approach at 7T, patients with

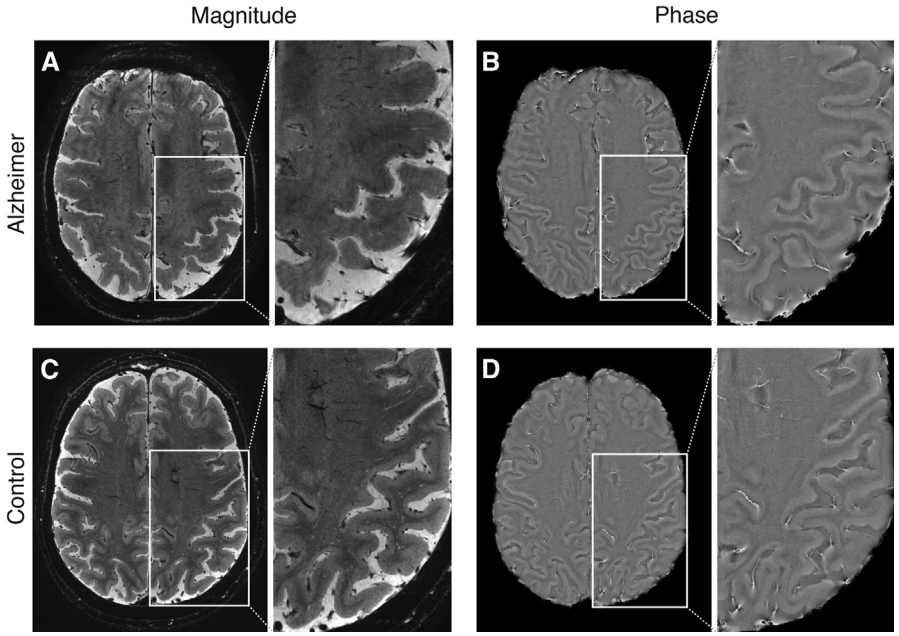

Fig. 2. (A–D) Representative 0.24 × 0.24-mm^2 two-dimensional T2*-weighted gradient echo images show a patient with Alzheimer's disease (A and B) and a control subject (C and D). (A and C) Magnitude images. (B and D) Phase images of the parietal cortex. No hypointense foci are seen on the magnitude images. The phase images show that the contrast between gray and white matter is enhanced in the patient with Alzheimer's disease in comparison with the control subject, indicating a larger cortical phase shift. Images show transverse planes.

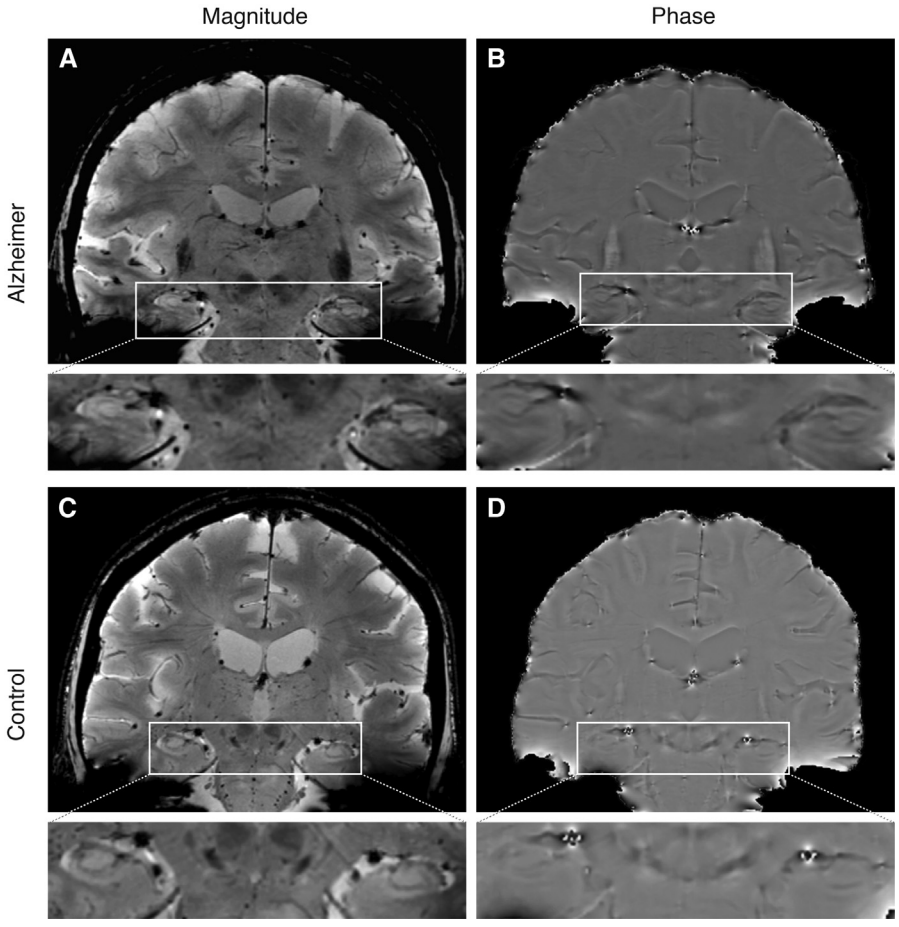

Fig. 3. (A–D) Representative 0.5 × 0.5-mm^2 two-dimensional T2*-weighted gradient echo images show a patient with Alzheimer's disease (A and B) and a control subject (C and D). (A and C) Magnitude images. (B and D) Phase images of the hippocampus. No hypointense foci are seen on the magnitude images. The phase images show no difference between the patient with Alzheimer's disease and the control subject in terms of image contrast between the hippocampus and white matter.

clinical symptoms of AD demonstrate an increased cortical phase shift on T2*-weighted images. These phase shifts between AD patients and control subjects have a high specificity, independent of age and gender. Moreover, these phase shifts correlated with individual MMSE scores. Of all cortical areas studied, the parietal cortex shows the highest specificity combined with the highest sensitivity for the diagnosis of AD and the strongest correlation with MMSE score. On the other hand, phase shifts in the hippocampus were not significantly increased in AD patients and did not correlate with MMSE score.

High-field T2*-weighted MRI sequences are highly sensitive for iron deposits in the brain [37]. In autopsy material of AD patients, amyloid deposition and neurofibrillary tangles as well as tau deficiency were found to colocalize with neuronal iron accumulation [38–40]. Therefore, it is likely that the increased cortical phase shift found on high-field T2*-weighted MRI in patients with AD indirectly reflect AD pathology. Our data also show that the particular distribution of the phase changes in the brain follows the known cerebral distribution of amyloid deposition in AD. In our data, the neocortex—and more specifically, the parietal lobes—allowed much better differentiating of AD patients from control subjects based on phase shift compared with the hippocampus. In histological studies, it has been demonstrated that the neocortex is the first structure in the brain that is affected by amyloid depositions, whereas the hippocampus is not only more mildly affected by amyloid

Table 2
Mean phase shifts and standard deviations (SD) of the cortical and hippocampal subregions in AD patients and control subjects

Region	AD, rad (n = 16)	Control, rad (n = 15)	*P* value
Temporoparietal left	0.90 ± 0.08	0.79 + 0.08	**.001**
Temporoparietal right	0.97 + 0.10	0.85 + 0.09	**.001**
Frontal	0.70 ± 0.08	0.62 ± 0.07	**.004**
Parietal	0.87 ± 0.10	0.74 ± 0.08	**.000**
Hippocampus right	0.09 ± 0.04	0.07 ± 0.03	.18
Hippocampus left	0.10 ± 0.04	0.08 ± 0.02	.14

Abbreviation: AD, Alzheimer's disease; rad, radians.
NOTE: Boldface values denote statistical significance.

Table 3
Area under the curve (AUC), cutoff value, sensitivity, specificity, positive predictive value (PPV+), and negative predictive value (NPV−) of phase shifts in differentiating between Alzheimer's disease patients and control subjects for the different regions

Region	AUC	Cutoff value, rad	Sensitivity, %	Specificity, %	PPV+, %	NPV−, %
Temporoparietal, left	0.842	0.922	56 (9/16)	100 (15/15)	100 (9/9)	68 (15/22)
Temporoparietal, right	0.823	0.985	50 (8/16)	100 (15/15)	100 (8/8)	65 (15/23)
Frontal	0.794	0.690	56 (9/16)	93 (14/15)	90 (9/10)	67 (14/21)
Parietal	0.854	0.817	69 (11/16)	93 (14/15)	92 (11/12)	74 (14/19)
Hippocampus, right	0.655	0.074	75 (9/12)	71 (10/14)	69 (9/13)	77 (10/13)
Hippocampus, left	0.673	0.095	58 (7/12)	86 (12/14)	78 (7/9)	71 (12/17)

Abbreviation: rad, radians.

plaques but is also affected at a later stage of AD than the neocortex [41–43]. This sequence of events has been confirmed by PiB-PET studies showing high amyloid loads in the parietal and frontal lobes and not in hippocampus [5–7,44,45]. However, phase shift changes might be caused by other factors than iron-bound plaques, such as iron itself or iron-bound CAA, but also by geometry and orientation. Therefore, the absence of phase shift changes in the hippocampus might, in part, be masked by geometric distortions.

Phase measurement on T2*-weighted MRI at 7T has a high specificity for AD compared with the reported specificity of the methods that are currently considered state of the art, such as cerebrospinal fluid (CSF) assay of the amyloid peptide or PiB-PET imaging [9]. Previous studies indicated that AD patients have reduced levels of $A\beta_{1–42}$ and increased levels of t-tau and p-tau_{181p} in CSF compared with control subjects, in whom $A\beta_{1–42}$ is the most sensitive biomarker for AD of CSF samples. 7T MRI had lower sensitivity than these CSF analyses of $A\beta_{1–42}$ (69% vs 96%), but had a higher specificity (93%–100% vs 77%) [46]. PET studies using PiB have shown the possibility of detecting cerebral amyloid accumulation, although the diagnostic utility is limited [47], and numbers on sensitivity and specificity are sparse. Mormino and colleagues [48] showed high sensitivity (90%) and specificity (90%) in differentiating AD patients from control subjects. However, within the group of healthy subjects, the specificity drops with increasing age, because the percentage of positive PiB-PET scans increases rapidly, with 12% of the people in their 60s, 30% in their 70s, and 50% in their 80s giving false-positive results [45,49,50]. Our data show that measurement of phase shift using T2*-weighted MRI might improve the specificity of AD diagnosis.

Our study could not replicate the ex vivo finding of hypointense foci, which might represent amyloid plaques [10]. Although we corrected for resonance frequency variations, which are the main contributor to decreased image quality in AD patients, with a navigator echo [34], it is highly likely that even subvoxel degrees of motion blur the hypointense foci.

A limitation of the current study is that phase measurements might also be influenced by the geometry and orientation of the scans [28]. We limited these effects as much as possible by positioning every participant carefully in the same manner. Moreover, phase values were measured in the exact same way using a standardized method. Furthermore, we averaged multiple measurements of phase values to cancel out the possible effects of geometry and orientation. A second limitation is that white matter phase values, which were used to correct for magnetic field inhomogeneities, might have an influence on the results. However, our data show that the observed phase changes were caused mainly by phase shifts in the gray matter. A third limitation is that we only included a relatively small number of AD patients and healthy control subjects, and therefore the sensitivity and specificity in general cannot be determined optimally, and the diagnostic accuracy in a group of memory clinic patients is unclear. The specificity of the presented method should be examined thoroughly by assessing different categories of neurodegenerative diseases to evaluate the ability to differentiate between different forms of dementia. Moreover, the value of our method should be investigated in the preclinical stages of AD. Therefore, in future studies we aim to study cortical phase changes in patients with mild cognitive impairment to evaluate the possibility of detecting early AD pathology and to evaluate the use of these cortical phase changes as an early treatment marker because the biological activity has already peaked before the symptomatic stage [1]. In addition, future studies should address translational research from 7T to 3T MRI to investigate whether our method could be used on 3T MRI data because 7T MRI is not widely available. Still, we expect that 7T will show larger phase shifts between AD patients and control subjects than 3T, as a direct result of the higher field strength.

In conclusion, in this study we introduced a novel approach to detect cortical changes in AD patients, exploiting the increased sensitivity of 7T MRI for iron in brain tissue. Our current data demonstrate that cortical phase changes are a potential new biomarker for AD.

Acknowledgments

This research was performed within the framework of CTMM, the Center for Translational Molecular Medicine (www.ctmm.nl), project LeARN (grant 02N-101) and was

supported by NGI/NWO (05040202, 050-060-810) and HEALTH-2007-2.4.5-10.

RESEARCH IN CONTEXT

1. Systematic review: We searched PubMed and ISI-Web of Knowledge for articles including Alzheimer's disease (AD), amyloid and AD pathology detection, high-field magnetic resonance imaging (MRI), phase measurements, cortical changes, biomarkers for AD, and brain imaging. Our research question evolved based on findings of our previous postmortem study on AD brain specimens.
2. Interpretation: In this study, we introduced a novel approach to detect cortical changes in AD patients exploiting the increased sensitivity of 7T MRI for iron in brain tissue. Our current data demonstrate that cortical phase changes are a potential new biomarker for AD.
3. Future directions: The diagnostic value and ability of our new approach as a biomarker for AD should be investigated further by expanding the inclusion of the number of AD patients and control subjects as well as include patients with mild cognitive impairment (preclinical stage of AD) and other dementias using 7T MRI and phase shift measurements.

References

[1] Nelson PT, Braak H, Markesbery WR. Neuropathology and cognitive impairment in Alzheimer disease: a complex but coherent relationship. J Neuropathol Exp Neurol 2009;68:1–14.
[2] Johnson KA, Gregas M, Becker JA, Kinnecom C, Salat DH, Moran EK, et al. Imaging of amyloid burden and distribution in cerebral amyloid angiopathy. Ann Neurol 2007;62:229–34.
[3] Lockhart A, Lamb JR, Osredkar T, Sue LI, Joyce JN, Ye L, et al. PIB is a non-specific imaging marker of amyloid-beta (Abeta) peptide-related cerebral amyloidosis. Brain 2007;130:2607–15.
[4] Ikonomovic MD, Klunk WE, Abrahamson EE, Mathis CA, Price JC, Tsopelas ND, et al. Post-mortem correlates of in vivo PiB-PET amyloid imaging in a typical case of Alzheimer's disease. Brain 2008; 131:1630–45.
[5] Klunk WE, Engler H, Nordberg A, Wang Y, Blomqvist G, Holt DP, et al. Imaging brain amyloid in Alzheimer's disease with Pittsburgh compound-B. Ann Neurol 2004;55:306–19.
[6] Engler H, Forsberg A, Almkvist O, Blomquist G, Larsson E, Savitcheva I, et al. Two-year follow-up of amyloid deposition in patients with Alzheimer's disease. Brain 2006;129:2856–66.
[7] Rowe CC, Ng S, Ackermann U, Gong SJ, Pike K, Savage G, et al. Imaging beta-amyloid burden in aging and dementia. Neurology 2007; 68:1718–25.
[8] Bacskai BJ, Frosch MP, Freeman SH, Raymond SB, Augustinack JC, Johnson KA, et al. Molecular imaging with Pittsburgh compound B confirmed at autopsy: a case report. Arch Neurol 2007;64:431–4.
[9] Rowe CC, Villemagne VL. Brain amyloid imaging. J Nucl Med 2011;52:1733–40.
[10] van Rooden S, Maat-Schieman ML, Nabuurs RJ, van der Weerd L, van Duijn S, van Duinen SG, et al. Cerebral amyloidosis: postmortem detection with human 7.0-T MR imaging system. Radiology 2009; 253:788–96.
[11] Benveniste H, Einstein G, Kim KR, Hulette C, Johnson GA. Detection of neuritic plaques in Alzheimer's disease by magnetic resonance microscopy. Proc Natl Acad Sci U S A 1999;96:14079–84.
[12] Zhang J, Yarowsky P, Gordon MN, Di Carlo G, Munireddy S, van Zijl PC, et al. Detection of amyloid plaques in mouse models of Alzheimer's disease by magnetic resonance imaging. Magn Reson Med 2004;51:452–7.
[13] Helpern JA, Lee SP, Falangola MF, Dyakin VV, Bogart A, Ardekani B, et al. MRI assessment of neuropathology in a transgenic mouse model of Alzheimer's disease. Magn Reson Med 2004;51:794–8.
[14] Lee SP, Falangola MF, Nixon RA, Duff K, Helpern JA. Visualization of beta-amyloid plaques in a transgenic mouse model of Alzheimer's disease using MR microscopy without contrast reagents. Magn Reson Med 2004;52:538–44.
[15] Jack CR Jr, Garwood M, Wengenack TM, Borowski B, Curran GL, Lin J, et al. In vivo visualization of Alzheimer's amyloid plaques by magnetic resonance imaging in transgenic mice without a contrast agent. Magn Reson Med 2004;52:1263–71.
[16] Braakman N, Matysik J, van Duinen SG, Verbeek F, Schliebs R, de Groot HJ, et al. Longitudinal assessment of Alzheimer's beta-amyloid plaque development in transgenic mice monitored by in vivo magnetic resonance microimaging. J Magn Reson Imaging 2006;24:530–6.
[17] Vanhoutte G, Dewachter I, Borghgraef P, Van Leuven F, Van der Linden A. Noninvasive in vivo MRI detection of neuritic plaques associated with iron in APP[V717I] transgenic mice: a model for Alzheimer's disease. Magn Reson Med 2005;53:607–13.
[18] Nakada T, Matsuzawa H, Igarashi H, Fujii Y, Kwee IL. In vivo visualization of senile-plaque-like pathology in Alzheimer's disease patients by MR microscopy on a 7T system. J Neuroimaging 2008; 18:125–9.
[19] Meadowcroft MD, Connor JR, Smith MB, Yang QX. MRI and histological analysis of beta-amyloid plaques in both human Alzheimer's disease and APP/PS1 transgenic mice. J Magn Reson Imaging 2009; 29:997–1007.
[20] Falangola MF, Lee SP, Nixon RA, Duff K, Helpern JA. Histological co-localization of iron in Abeta plaques of PS/APP transgenic mice. Neurochem Res 2005;30:201–5.
[21] Grundke-Iqbal I, Fleming J, Tung YC, Lassmann H, Iqbal K, Joshi JG. Ferritin is a component of the neuritic (senile) plaque in Alzheimer dementia. Acta Neuropathol 1990;81:105–10.
[22] El Tannir, El Tayara N, Delatour B, Le Cudennec C, Guegan M, Volk A, Dhenain M. Age-related evolution of amyloid burden, iron load, and MR relaxation times in a transgenic mouse model of Alzheimer's disease. Neurobiol Dis 2006;22:199–208.
[23] Exley C. Aluminium and iron, but neither copper nor zinc, are key to the precipitation of beta-sheets of Abeta_{42} in senile plaque cores in Alzheimer's disease. J Alzheimers Dis 2006;10:173–7.
[24] Lovell MA, Robertson JD, Teesdale WJ, Campbell JL, Markesbery WR. Copper, iron and zinc in Alzheimer's disease senile plaques. J Neurol Sci 1998;158:47–52.
[25] Ogg RJ, Langston JW, Haacke EM, Steen RG, Taylor JS. The correlation between phase shifts in gradient-echo MR images and regional brain iron concentration. Magn Reson Imaging 1999;17:1141–8.
[26] Haacke EM, Cheng NY, House MJ, Liu Q, Neelavalli J, Ogg RJ, et al. Imaging iron stores in the brain using magnetic resonance imaging. Magn Reson Imaging 2005;23:1–25.
[27] Haacke EM, Ayaz M, Khan A, Manova ES, Krishnamurthy B, Gollapalli L, et al. Establishing a baseline phase behavior in magnetic resonance imaging to determine normal vs. abnormal iron content in the brain. J Magn Reson Imaging 2007;26:256–64.

[28] Yao B, Li TQ, van Gelderen P, Shmueli K, de Zwart JA, Duyn JH. Susceptibility contrast in high field MRI of human brain as a function of tissue iron content. Neuroimage 2009;44:1259–66.
[29] Duyn JH, van Gelderen P, Li TQ, de Zwart JA, Koretsky AP, Fukunaga M. High-field MRI of brain cortical substructure based on signal phase. Proc Natl Acad Sci U S A 2007;104:11796–801.
[30] Fukunaga M, Li TQ, van Gelderen P, de Zwart JA, Shmueli K, Yao B, et al. Layer-specific variation of iron content in cerebral cortex as a source of MRI contrast. Proc Natl Acad Sci U S A 2010;107:3834–9.
[31] Lynoe N, Sandlund M, Dahlqvist G, Jacobsson L. Informed consent: study of quality of information given to participants in a clinical trial. BMJ 1991;303:610–3.
[32] McKhann G, Drachman D, Folstein M, Katzman R, Price D, Stadlan EM. Clinical diagnosis of Alzheimer's disease: report of the NINCDS-ADRDA Work Group under the auspices of Department of Health and Human Services Task Force on Alzheimer's Disease. Neurology 1984;34:939–44.
[33] Greenberg SM. Cerebral amyloid angiopathy: prospects for clinical diagnosis and treatment. Neurology 1998;51:690–4.
[34] Versluis MJ, Peeters JM, van Rooden S, van der Grond J, van Buchem MA, Webb AG, et al. Origin and reduction of motion and f0 artifacts in high resolution T2*-weighted magnetic resonance imaging: application in Alzheimer's disease patients. Neuroimage 2010; 51:1082–8.
[35] Schar M, Kozerke S, Fischer SE, Boesiger P. Cardiac SSFP imaging at 3 Tesla. Magn Reson Med 2004;51:799–806.
[36] Haacke EM, Xu Y, Cheng YC, Reichenbach JR. Susceptibility weighted imaging (SWI). Magn Reson Med 2004;52:612–8.
[37] Duyn JH. The future of ultra-high field MRI and fMRI for study of the human brain. Neuroimage 2011;62:1241–8.
[38] Duce JA, Tsatsanis A, Cater MA, James SA, Robb E, Wikhe K, et al. Iron-export ferroxidase activity of beta-amyloid precursor protein is inhibited by zinc in Alzheimer's disease. Cell 2010;142:857–67.
[39] Lei P, Ayton S, Finkelstein DI, Spoerri L, Ciccotosto GD, Wright DK, et al. Tau deficiency induces parkinsonism with dementia by impairing APP-mediated iron export. Nat Med 2012;18:291–5.
[40] Smith MA, Harris PL, Sayre LM, Perry G. Iron accumulation in Alzheimer disease is a source of redox-generated free radicals. Proc Natl Acad Sci U S A 1997;94:9866–8.
[41] Braak H, Braak E. Neuropathological staging of Alzheimer-related changes. Acta Neuropathol 1991;82:239–59.
[42] Arnold SE, Hyman BT, Flory J, Damasio AR, Van Hoesen GW. The topographical and neuroanatomical distribution of neurofibrillary tangles and neuritic plaques in the cerebral cortex of patients with Alzheimer's disease. Cereb Cortex 1991;1:103–16.
[43] Thal DR, Rub U, Orantes M, Braak H. Phases of A beta-deposition in the human brain and its relevance for the development of AD. Neurology 2002;58:1791–800.
[44] Ng SY, Villemagne VL, Masters CL, Rowe CC. Evaluating atypical dementia syndromes using positron emission tomography with carbon 11 labeled Pittsburgh compound B. Arch Neurol 2007; 64:1140–4.
[45] Mintun MA, Larossa GN, Sheline YI, Dence CS, Lee SY, Mach RH, et al. [11C]PIB in a nondemented population: potential antecedent marker of Alzheimer disease. Neurology 2006;67:446–52.
[46] Shaw LM, Vanderstichele H, Knapik-Czajka M, Clark CM, Aisen PS, Petersen RC, et al. Cerebrospinal fluid biomarker signature in Alzheimer's Disease Neuroimaging Initiative subjects. Ann Neurol 2009;65:403–13.
[47] Quigley H, Colloby SJ, O'Brien JT. PET imaging of brain amyloid in dementia: a review. Int J Geriatr Psychiatry 2011;26:991–9.
[48] Mormino EC, Kluth JT, Madison CM, Rabinovici GD, Baker SL, Miller BL, et al. Episodic memory loss is related to hippocampal-mediated beta-amyloid deposition in elderly subjects. Brain 2009; 132:1310–23.
[49] Rowe CC, Ellis KA, Rimajova M, Bourgeat P, Pike KE, Jones G, et al. Amyloid imaging results from the Australian Imaging, Biomarkers and Lifestyle (AIBL) Study of Aging. Neurobiol Aging 2010; 31:1275–83.
[50] Villemagne VL, Pike KE, Chetelat G, Ellis KA, Mulligan RS, Bourgeat P, et al. Longitudinal assessment of Abeta and cognition in aging and Alzheimer disease. Ann Neurol 2011;69:181–92.